

Fuel Efficiency Analysis and Control of a Series Electric Hybrid Compact Wheel Loader

Mohamed Allam,^{1,2} Orlando Fernandez,¹ and Matti Linjama¹

¹Tampere University, Faculty of Engineering and Natural Sciences, Finland

²Ain Shams University, Faculty of Engineering, Egypt

Abstract

The escalating demand for more efficient and sustainable working machines has pushed manufacturers toward adopting electric hybrid technology. Electric powertrains promise significant fuel savings, which are highly dependent on the nature of the duty cycle of the machine. In this study, experimental data measured from a wheel loader in a short-loading Y-cycle is used to exercise a developed mathematical model of a series electric hybrid wheel loader. The efficiency and energy consumption of the studied architecture are analyzed and compared to the consumption of the measured conventional machine that uses a diesel engine and a hydrostatic transmission. The results show at least 30% reduction in fuel consumption by using the proposed series electric hybrid powertrain, the diesel engine rotational speed is steady, and the transient loads are mitigated by the electric powertrain. The model also shows that 20% of drive energy could be regenerated through braking using the drive electric motors. Opportunities for engine downsizing are established and the losses are analyzed and compared for both machines. The results show 42% savings in the overall system losses especially the diesel engine and drivetrain.

History

Received: 27 Oct 2023
 Revised: 01 Feb 2024
 Accepted: 19 Mar 2024
 e-Available: 03 May 2024

Keywords

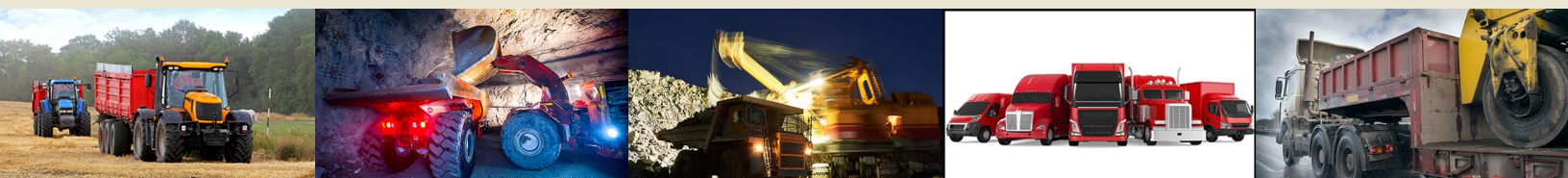
Powertrain, Series hybrid, Modeling, Heavy-duty equipment, Wheel loader

Citation

Allam, M., Fernandez, O., and Linjama, M., "Fuel Efficiency Analysis and Control of a Series Electric Hybrid Compact Wheel Loader," *SAE Int. J. Commer. Veh.* 17(2):197-211, 2024, doi:10.4271/02-17-02-0012.

ISSN: 1946-391X
 e-ISSN: 1946-3928

© 2024 Mohamed Allam, Orlando Delgado Fernandez, Matti Linjama; Published by SAE International. This Open Access article is published under the terms of the Creative Commons Attribution License (<http://creativecommons.org/licenses/by/4.0/>), which permits distribution, and reproduction in any medium, provided that the original author(s) and the source are credited.



I. Introduction

Wheel loaders are used to handle and transfer massive loads, including construction, mining, and earthwork applications. These machines usually rely on diesel engines, which consume significant amount of fuel due to the nature of the work they do. For example, some equipment may be used to haul loads of several tons on steep inclines, which leads to consumption ranging from 10,000 to 100,000 L of fuel per year per machine [1]. In addition to the high fuel consumption, they also experience significant energy losses due to unfavorable diesel engine operation (high loads and low speeds). In addition to that, the diesel engine efficiency is 40% at its highest while at normal operating conditions it is usually even less, which leads to deteriorated operation efficiency.

Numerous studies have been conducted to improve wheel loaders' efficiency and reduce their consumption and emissions, for example, reducing the speed of the engine [2] and use of hybrid hydraulics [3]. However, better fuel consumption can be achieved using electric hybrid powertrains. The integration of electric hybrid powertrains in heavy-duty machines not only reduces fuel consumption and emissions but also addresses the issue of energy losses and improves overall efficiency. An electric hybrid powertrain combines two or more prime movers, such as a battery and a diesel engine. This technology has shown to reduce fuel consumption by about 25%, as claimed by Hitachi and Caterpillar [4, 5] and up to 45% as claimed by Komatsu [6].

Hybrid electric powertrains can be constructed with different topologies such as the series, parallel, and series-parallel hybrid. Series hybrid powertrains operate the diesel engine at its peak efficiency, are simple in construction, and are easy to control but offer poor transmission efficiency due to several energy conversions. On the other hand, parallel hybrids provide high transmission efficiency, as it has less energy conversions and are more reliable. However, they operate the diesel engine at a lower efficiency zone. Finally, series-parallel hybrids offer the same advantages as parallel hybrids and operate the diesel engine at high efficiency but are more complicated in control and construction [7].

In this work, the series electric hybrid (SEH) powertrain technology is studied since it utilizes electric motors to handle the different power consumers, such as traction and hydraulic systems, while the diesel engine is decoupled from the mechanical load and its transients and is solely used to charge the battery pack through a generator. This enables efficient use of energy, provides optimal performance for different operating conditions, and opens the possibility to downsize the diesel engine where there is no more need for it to handle power peaks. Although the initial cost of the SEH powertrain is high compared to traditional and other hybrid machines, the long-term cost savings and environmental benefits make it a viable option for wheel loaders.

A large body of literature exists on simulation and control for hybrid electric powertrains in passenger cars. For example, multiple studies [8, 9, 10] introduced control strategies for

SEH vehicles using standardized urban driving cycles. Also, Chen et al. [11] proposed a strategy to optimize the driving speed simultaneously with the energy power source split for a SEH vehicle. Another research by Katrasnik et al. [12] presented a simulation and an analytical approach to find more insights into the energy conversion in hybrid powertrains. Finally, Evangelou et al. [13] presented a complete simulation model of a SEH car and is simulated using standardized driving cycle.

The standardized driving cycles for passenger cars, however, cannot be adapted for heavy-duty equipment since their duty cycles are significantly different, the abundance of transient loads from the equipment used by the machines such as heavy digging, lifting, and moving of massive loads are some examples. Heavy-duty equipment also contains components that are not common in passenger cars such as hydraulic pumps. These additional components add to the complexity of the system and differentiate it from passenger cars.

Fewer studies have focused on SEH powertrains in heavy-duty equipment. For example, in on-road equipment such as buses. Hu et al. [14] introduced a tank-to-wheel analysis of a series plug-in hybrid electric bus using different management strategies as well as battery sizes. Peng et al. [15] presented a rule-based energy management strategy for a plug-in hybrid bus. While for offroad heavy-duty equipment, Wang et al. [16] concluded that a powertrain topology for hydraulic excavators is cycle dependent where a parallel topology is suited for heavy and light use and a series or parallel is efficient for medium use.

Although these studies present fuel consumption optimization results for their respective machine, they cannot be directly extended for wheel loaders or generalized for heavy-duty equipment, due to the substantial difference in the duty cycle and operating conditions between different machines. For example, wheel loaders experience transient loading conditions as opposed to passenger cars or buses and their duty cycle is different from excavators as they have motion unlike excavators that are mostly stationary.

Few studies investigated the analysis of wheel loaders' SEH powertrains. For instance, Lin et al. [17] provided a battery power-based strategy for a SEH wheel loader showing a possibility of 43.6% fuel savings. Meanwhile, Tebaldi et al. [18] used power-oriented graphs to design a controller for the power management problem. Finally, Donato et al. [19] presented an evaluation of the benefit of hybridization of a compact wheel loader using a backward simulation model and a duty cycle provided by an industry partner. However, these studies rely on simplified duty cycles made for simulations, which neglect the transient data and the actual operating conditions that are critical to accurate fuel consumption estimation.

In this study, the fuel consumption of a SEH purpose-built wheel loader was studied and analyzed. Results were compared to a conventional wheel loader that uses a diesel engine and a hydrostatic transmission (HST). The two architectures were compared using data, which was experimentally measured from the conventional machine performing a Y-cycle. The data includes measurements from the diesel

engine, HST, and working and auxiliary hydraulics pumps. The comparison was performed using a formulated backward-facing MATLAB/Simulink model of the 5.4-ton SEH wheel loader; the model simulates the dynamics of different components of the powertrain to study the power distribution and energy consumption as well as the efficiency of the overall machine. The results for fuel consumption and energy losses are analyzed. Opportunities for improving the efficiency of the components are identified as well as the possibilities of energy regeneration through the electric motors and the downsizing of diesel engines are investigated. This study focuses on addressing the fuel consumption and efficiency challenges in diesel-powered wheel loaders, by exploring the potential of SEH powertrain to improve efficiency. The study presents an analysis of a purpose-built SEH wheel loader, comparing it with a conventional diesel-powered counterpart using real-world data.

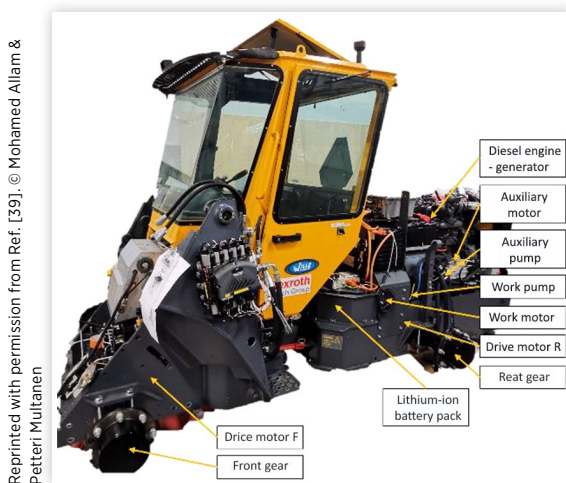
The article is organized as follows: [Section II](#) demonstrates the architecture of the studied powertrain. [Section III](#) discusses the modeling of the loader's components. [Section IV](#) presents the loading cycle. [Section V](#) shows the simulation model. [Section VI](#) summarizes results, and finally, [Section VII](#) contains the conclusions and future work.

II. Systems Architecture

The machine of the study shown in [Figure 1](#) is a 5.4-ton SEH wheel loader equipped with a 91-kW diesel engine connected to a permanent magnet synchronous generator that supplies power to a lithium-ion battery. The battery in turn supplies power to four electric motors that are used to propel the wheel loader and drive the implements and auxiliaries pump, respectively.

The studied structure is illustrated in [Figure 2\(a\)](#). The powertrain management is done through a central power distribution unit (PDU). The working hydraulics and the auxiliary systems are powered by fixed displacement pumps

FIGURE 1 Series electric hybrid wheel loader of the study.

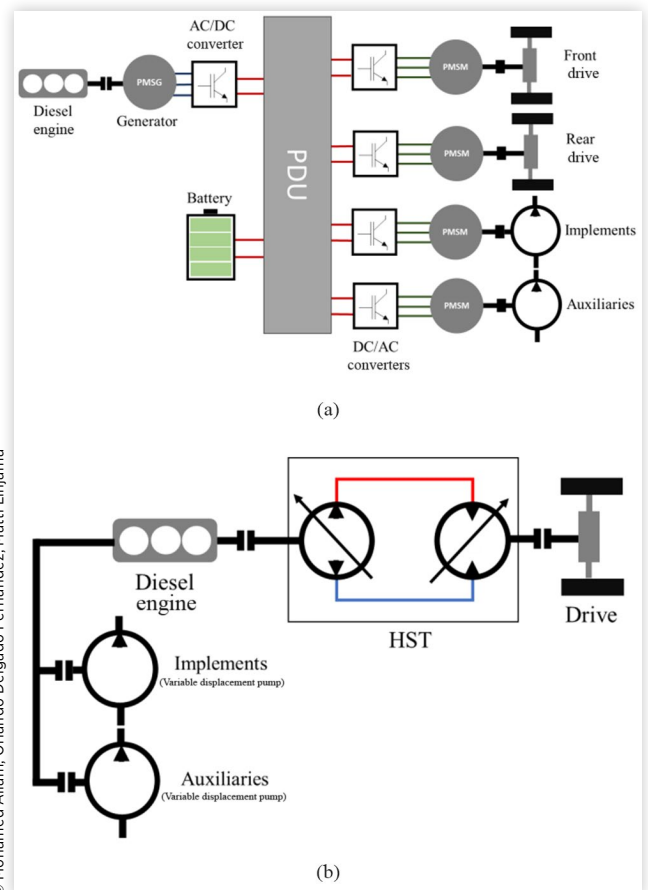


Reprinted with permission from Ref. [39]. © Mohamed Allam & Petteri Multanen

of capacity 48 cc and 4.5 cc, respectively. The conventional machine is illustrated in [Figure 2\(b\)](#), and it consists of an 83-kW diesel engine connected to a hydrostatic transmission (HST), which propels the wheels and two variable displacement pumps: one for the implements and the other for auxiliaries (63 cc and 26 cc). Other systems such as the hydraulic cylinders and valves for the lift and tilt functions are not considered in this study. The SEH wheel loader of the study is currently under construction at Tampere university. The machine is a part of a consortium of companies and research organizations developing new low-carbon products to meet the 2035 greenhouse gas regulations. The machine will function as a research platform for component optimization, energy-efficient control of hydraulics, development of power management strategies for the powertrain and thermal management, and analysis of electric components such as motors, generators, and the electrical storage system.

The SEH architecture was chosen as wheel loaders tend to operate at low speeds and high torques due to the nature of the working cycle [20], for example, a Y-cycle or a V-cycle. Moreover, wheel loaders usually spend most of their time idling with frequent starts and stops [7], which dictates a system that can operate the engine at its most efficient region [21].

FIGURE 2 Powertrain of the studied wheel loaders: (a) series electric hybrid wheel loader; (b) conventional diesel-powered wheel loader.



© Mohamed Allam, Orlando Delgado Fernandez, Matti Linjama

The SEH powertrain decouples the diesel engine from the operating condition transients, which gives the freedom to control the engine efficiently or turn it off completely.

III. Component Modeling

A. Diesel Engine

There are numerous approaches to internal combustion engine modeling such as filling and emptying models of zero and n-dimensional, quasi-linear or mean value models, and linear or sampled data modeling [22]. Although the first two provide (1) a more accurate insight into engine performance as they model the engine internals, (2) can predict engine response and its submodels, and (3) are suitable for transient performance prediction, they are computationally heavy and require detailed specifications of several diesel engine components, which are difficult to obtain. Since the SEH powertrain decouples the engine from the load transients, therefore, the diesel engine is modeled using a nonlinear efficiency map model using the torque and speed as inputs to calculate the efficiency.

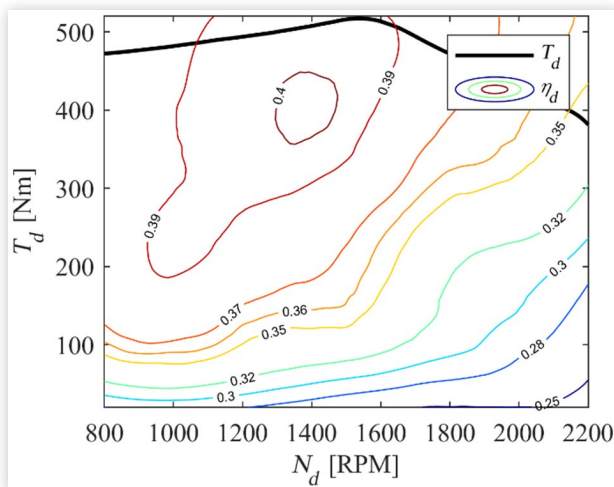
The model calculates the mechanical power of the engine shaft from the speed and torque values. The engine required power is then calculated through the efficiency chart where the required input power P_{in} is calculated from:

$$P_{in} = \frac{P_{out}}{\eta_d} \quad \text{Eq. (1)}$$

where $P_{out} = T_d \omega_d$ is the diesel engine crankshaft output power, T_d , ω_d are the output torque and rotational speed, and η_d is the diesel engine efficiency calculated from the efficiency map. The fuel consumption is calculated in L/hr using:

$$\dot{V}_f = \frac{3600 P_{in}}{E \rho} \quad \text{Eq. (2)}$$

FIGURE 3 Diesel engine power, torque, and efficiency against engine rotational speed.



Data taken from Ref. [23]. © Mohamed Allam, Orlando Delgado Fernandez, Matti Linjama

where E is the heating value of diesel fuel and ρ is diesel fuel density. The efficiency map for the engine is shown in [Figure 3](#) and is adapted from [23] and fitted to the studied machine diesel engine.

B. Electric Machines

The electrical machines (EMs) in the wheel loader are all three-phase permanent magnet synchronous motors/generators (PMSM/Gs). The modeling of such machines is achieved by representation in the d–q frame. This involves transforming the three-phase motor currents into two orthogonal axes: the d-axis, which is aligned with the magnetic field of the rotor, and the q-axis, which is perpendicular to the d-axis. This transformation allows for decoupling of the motor's electrical and magnetic dynamics, making it easier to control.

The motor is then controlled by adjusting the voltage and current in the d- and q-axes using a proportional–integral (PI) controller, which calculates the required voltages to maintain the desired torque and speed, where changing the q-axis current while keeping the d-axis current to zero maximizes the torque. The d-axis current can be driven negative to optimize the flux to implement field weakening to operate above nominal speed.

The equations for PMSM consist of a mechanical and an electrical component where the d-axis voltage is v_d given by [24]:

$$v_d = \frac{di_d}{dt} L_d + Ri_d - L_q P \omega_m i_q \quad \text{Eq. (3)}$$

where i_d , L_d are the d-axis current and inductance, R is the winding resistance, P is the number of pole pairs of the PMSM, ω_m is the motor's angular mechanical speed, and the q-axis voltage v_q is denoted by:

$$v_q = \frac{di_q}{dt} L_q + Ri_q + L_d P \omega_m i_d + \lambda_m P \omega_m \quad \text{Eq. (4)}$$

where i_q , L_q are the q-axis current and inductance and λ_m is the motor's magnetic flux linkage constant.

The machine torque T_e is calculated from [25]:

$$T_e = \frac{3}{2} P \left(\lambda_m i_q + (L_d - L_q) i_d i_q \right) \quad \text{Eq. (5)}$$

and the electrical angular velocity ω_e of the motor is:

$$\omega_e = P \omega_m \quad \text{Eq. (6)}$$

and for the mechanical system:

$$T_e - T_L - F \omega_m = J \frac{d\omega}{dt} \quad \text{Eq. (7)}$$

where T_L is the motor load torque, F is the coefficient of viscous friction, and J is the equivalent inertia of the electric machine and attachments.

The parameters of the EMs used in the model are adapted from the manufacturer's datasheets.

C. Battery

The electrical energy storage consists of seven lithium-ion battery packs connected in series. All the cells are assumed to have uniform behavior with an equal temperature distribution across all cells. The battery pack voltage v_{DC} is calculated as:

$$v_{DC} = n_c v_t \quad \text{Eq. (8)}$$

where n_c is the number of cells and v_t is each cell's terminal voltage.

The battery is simulated as an equivalent circuit model (ECM) illustrated in [Figure 4](#) with six pairs of resistance–capacitance (RC) circuits along with a thermal model.

This allows the model to capture the static and dynamic behavior of the battery during charging and discharging [26]. The model uses the required current as input, and the output is the current state of charge (SOC), battery's terminal voltage, power losses, and temperature.

The ECM consists of an ideal voltage source representing the SOC and the resting behavior of the cell, an internal resistor that describes what happens when the cell is subject to a time-varying input current, and a series of RC circuits that represent the slow diffusion process of lithium (diffusion voltage). Unlike the diesel engine the battery is subject to highly dynamic current input and its performance varies accordingly; hence, these dynamics must be modeled where they are represented by the following equations, where battery's terminal voltage v_t is calculated from the voltage drop across the internal resistor as well as the RC circuits:

$$v_t = \text{OCV}(t, \text{SOC}) - i(t)R_o - v_{c_n}(t) \quad \text{Eq. (9)}$$

where open circuit voltage (OCV) is the battery's open circuit voltage, which is a function of SOC, R_o is the battery's internal resistance, v_{c_n} is the voltage drop across the RC circuits, and n denotes the number of RC circuit.

The current through the RC circuit is calculated from:

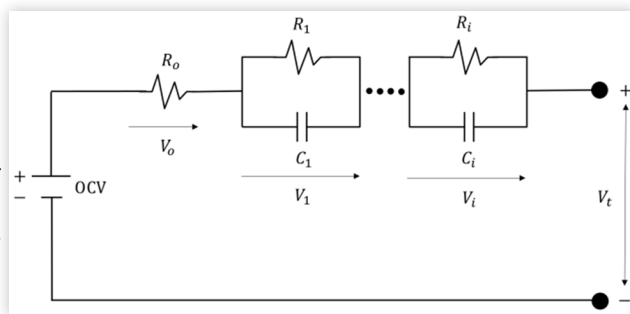
$$i_{R_n}(t) + C_n \dot{v}_{c_n}(t) = i(t) \quad \text{Eq. (10)}$$

where C_n is the capacitance of the RC circuit, since $v_{c_n} = R_n i_{R_n}(t)$, the current through the RC circuit can be calculated from:

$$i_{R_n} = \frac{1}{R_n C_n} \int (i(t) - i_{R_n}(t)) \quad \text{Eq. (11)}$$

where R_n is the resistance of the RC circuit.

FIGURE 4 Equivalent circuit model for one cell.



© Mohamed Allam, Orlando Deigado Fernandez, Matti Linjama

To study the efficiency of the battery, power losses are calculated where:

$$P_l = n_c \left(i(t)^2 R_o + \sum_1^n \frac{v_{c_n}^2}{R_n} \right) \quad \text{Eq. (12)}$$

and the SOC of the battery is calculated using coulomb counting from:

$$\text{SOC}(t) = \text{SOC}_o - \int_{t_o}^t \frac{i(\tau)}{3600 * Q} d\tau \quad \text{Eq. (13)}$$

where SOC_o is the initial SOC, Q is the battery capacity, and i is the current.

Finally, the temperature of the battery's cell T is calculated from [27]:

$$C_T \frac{dT}{dt} = \frac{T - T_a}{R_T} + P_l \quad \text{Eq. (14)}$$

where C_T is the battery cell heat capacitance, T_a is the ambient air temperature, and R_T is the convection resistance.

The parameters of the ECM and the thermal model were estimated using MATLAB parameter estimation through a pulse discharge test. An estimation for one pulse is shown in [Figure 5\(a\)](#), and the response of the terminal voltage for one cell using the estimated parameters is shown in [Figure 5\(b\)](#).

The parameter estimation was done on all pulses representing different SOC's where the parameters vary with different SOC. The methodology followed for parameter estimation is derived from [28] where the resistance and capacitance of the RC circuits are functions of the SOC:

$$R_n = f(\text{SOC}) \quad \text{Eq. (15)}$$

$$C_n = f(\text{SOC}) \quad \text{Eq. (16)}$$

The OCV versus the SOC relation was adapted from the manufacturers' data sheet and is shown in [Figure 6](#).

D. AC/DC Converter

The converter transfers the power from the electric motors and the generator and then outputs the current that is used to discharge or recharge the battery according to the drive cycle information. The electric motors' AC power is calculated from [24]:

$$P_m = \frac{3}{2} (v_d i_d + v_q i_q) \quad \text{Eq. (17)}$$

The total power discharged from the lithium-ion battery having a terminal voltage v_t is:

$$P_b = v_t i \quad \text{Eq. (18)}$$

Since the AC and DC powers are almost equal, the capacitance of the DC bus is neglected, and the net current required can be calculated from:

$$i = \frac{P_m}{v_t \eta_c} \quad \text{Eq. (19)}$$

where η_c is the converter efficiency, which was assumed to be constant at 0.98.

FIGURE 5 Battery parameter estimation: (a) parameter estimation using a pulse discharge test (single pulse); (b) battery's terminal voltage to 20% SOC using the estimated parameters.

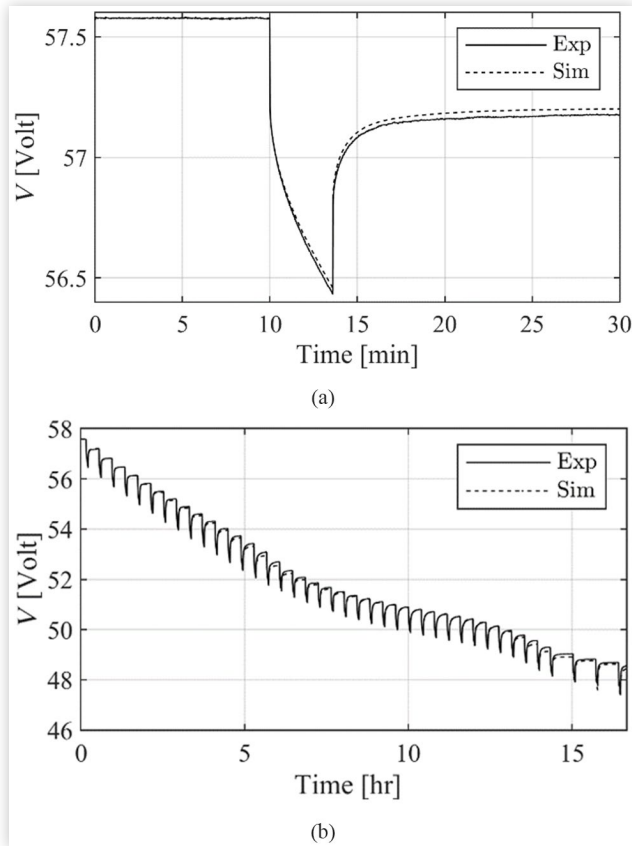
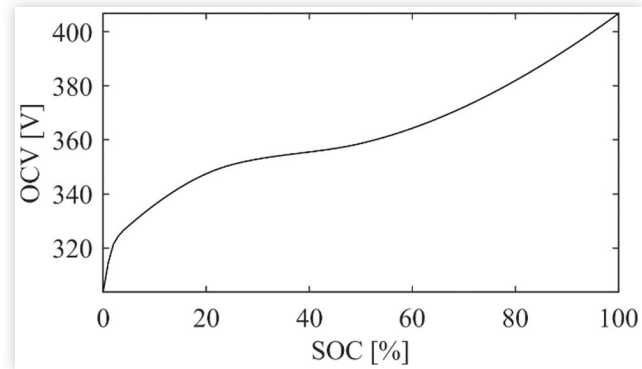


FIGURE 6 Open circuit voltage vs SOC relationship at 25°C.



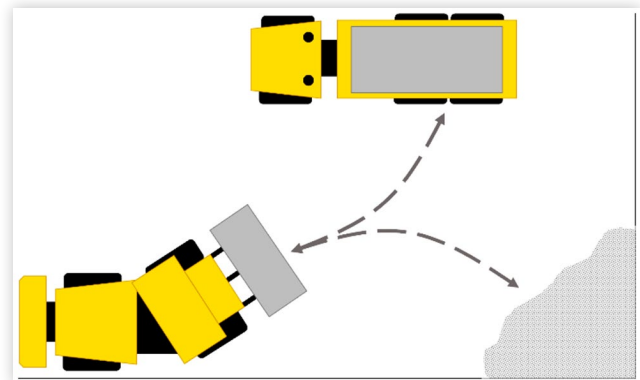
© Mohamed Allam, Orlando Delgado Fernandez, Matti Linjama

IV. Duty Cycle

Wheel loaders operate in a variety of applications such as material handling, stockpiling, and excavation. The two most common operating cycles include the short-loading Y-cycle and the load and carry cycle [30, 31]. Both provide accurate representation of the wheel loader's operating conditions since they include the operation of all machine's systems such as drive, implements, steering, and braking. The Y-cycle is chosen for this study as experimental measurements are available from the conventional machine defining the loads for the SEH loader. Although additional cycles would improve the accuracy of the results, limitation on measured data availability makes it difficult. Duty cycles of wheel loaders are not standardized and documented as in passenger cars. In wheel loaders, it is required to measure several phenomena to generate a realistic cycle such as diesel engine speed, different pump's pressures and flow rates, and machine speed. On the other hand, for passenger cars only the measurement of vehicle speed is required to produce a duty cycle where many standardized cycles are available. The Y-cycle shown in Figure 7 of a wheel loader is a series of steps that the operator follows to load and transport materials.

It is named after the shape of the path that the loader follows during each cycle, which resembles the letter "Y."

FIGURE 7 Wheel loader Y-cycle under investigation.



© Mohamed Allam, Orlando Delgado Fernandez, Matti Linjama

E. Fixed Displacement Pumps

The pumps that operate the tilt, lift, steering, and braking are fixed displacement pumps that deliver a certain amount of fluid per revolution. There are different models to simulate the pump behavior, such as lossless models, efficiency models, and other models that use tabulation and curve fitting. In this work pumps are modeled considering both flow and torque losses, where the pump's flow rate is calculated from:

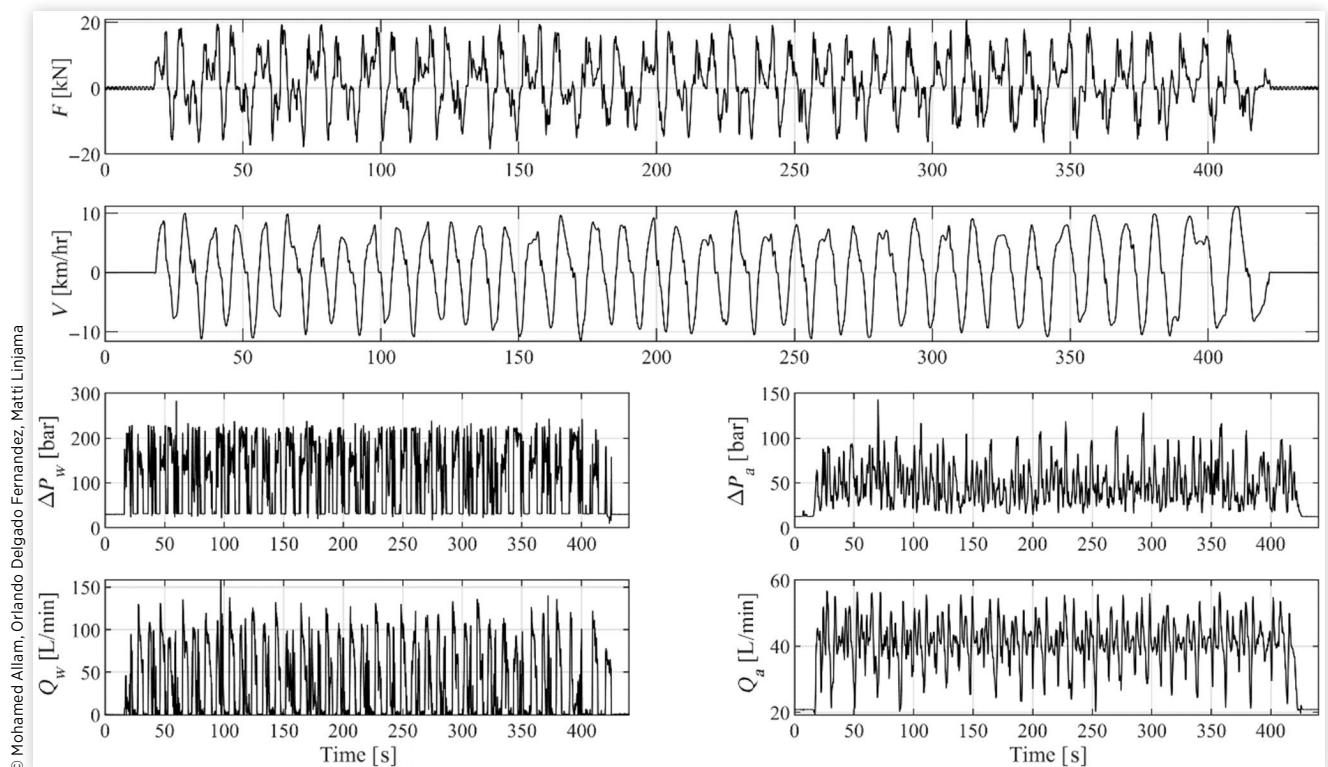
$$Q_p = \varepsilon_p V_p n_p - Q_{loss} \quad \text{Eq. (20)}$$

where ε_p is the pump setting [0,1], V_p is the pump's volumetric displacement, n_p is the rotational speed in rev/s.

The pump flow losses Q_{loss} are classified into leakage flow loss from the high-pressure outlet to the low-pressure outlet as well as friction torque. The pump torque can be deduced from [29]:

$$T_p = \frac{\varepsilon_p V_p \Delta P}{2\pi} + T_{loss} \quad \text{Eq. (21)}$$

where ΔP is the pressure difference across the pump.

FIGURE 8 The duty cycle measurements showing force, speed, working and auxiliaries pump pressures, and flow rates.

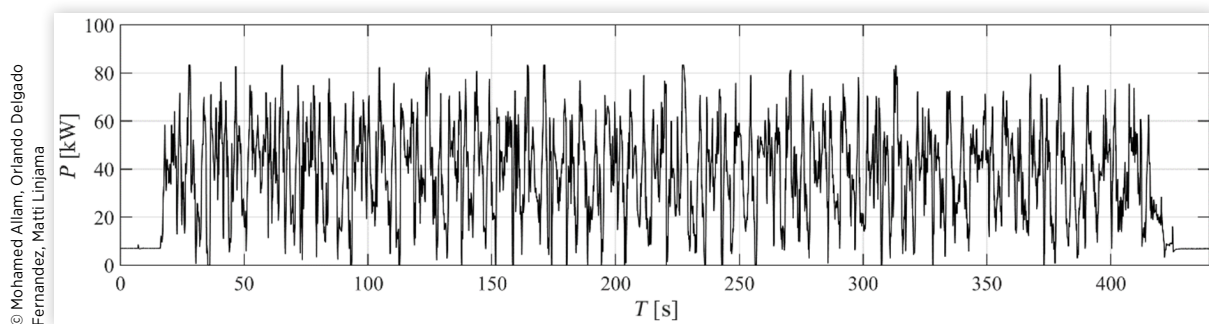
© Mohamed Allam, Orlando Delgado Fernandez, Matti Linjama

The steps of the Y-cycle start with the loader approaching the pile of material to be loaded. The boom is lowered, and the bucket is tilted to dig into the pile of material, filling to its capacity. Next, the bucket is tilted backward, and the boom is raised to a safe height and the loader is reversed and pivoted toward the dump position. After that, it moves toward the dump position and tilts the bucket downward to empty. Finally, the loader is reversed again usually while lowering the boom and tilting the bucket to the fill position. The cycle is repeated several times until the materials are moved [32].

The duty cycle information was recorded from a similar diesel conventional wheel loader executing the maneuver in real-time and is used as input to the simulation model to exercise the components and study their behavior. Figure 8 shows the measured drive force, machine speed, working and

auxiliaries pump pressures, and flow rates of the cycle. More details on the measurements and estimations can be found in Ref. [33]. The machine speed varies between 10 and -10 km/hr while the pump pressures vary between 10 and 210 bar with one peak at 283 bar for the work pump and between 12 and 100 bar with also one peak at 142 bar for the auxiliary pump. The peaks in the measurements represent some extreme conditions that the wheel loader is experiencing such as heavy digging, acceleration, or a combination of several loads at the same time. These conditions were intentionally included in the cycle to assess the performance of the SEH loader under extreme conditions beyond its typical operation.

The power of the diesel engine measured during the Y-cycle is shown in Figure 9 where the maximum power is at 83 kW.

FIGURE 9 Total diesel engine power required in the duty cycle.

© Mohamed Allam, Orlando Delgado Fernandez, Matti Linjama

V. Simulation

The model is a backward-facing simulation approach where the drive cycle information was measured in terms of traction force, machine speed, pumps' differential pressure, and flow rate. The data recorded from the drive cycle is converted to each component as input and propagated through the rest of the model to the battery as required power. The proposed flow of the model is shown in [Figure 10](#). The torque of the front and rear motors T_{ei} is calculated from:

$$T_{e_i} = \frac{F_{drive} r_w}{\eta_t i_f k_d} \quad \text{Eq. (22)}$$

where F_{drive} is the driving force calculated from the estimated HST power and the vehicle speed, r_w is the wheel radius, η_t is the transmission efficiency, i_f is the total reduction ratio of the powertrain, k_d is a distribution factor for the front and rear motors since the measurements are from a rear wheel drive loader. The input rotational speed ω_{ei} of the drive motors is also calculated from:

$$\omega_{e_i} = \frac{V_m i_f}{r_w} \quad \text{Eq. (23)}$$

where V_m is the measured speed. Finally, the electric motors' torque and speed for the work and auxiliaries' pumps are calculated using the pumps equations presented in [Section III](#). It is worth noting that phenomenon like the air resistance, rolling resistance, slipping, ground conditions, and rotating masses are included in the measurements adding a layer of accuracy to the simulation.

The diesel engine and generator speeds are controlled through a P controller that holds the battery's SOC at a threshold level, and the generator torque is set at its nominal value to minimize the losses and use the available power without overheating.

$$\omega_d \propto \text{SOC} \quad \text{Eq. (24)}$$

The parameters of the simulated model and components are shown in [Table 1](#).

VI. Results

The model is simulated using the recorded information from the Y-cycle where the diesel engine and the generator reference torque are set at 135 Nm, which is the generator nominal torque. The desired SOC is set at 80% and the initial SOC's for

FIGURE 10 Backward-facing simulation model of the SEH wheel loader.

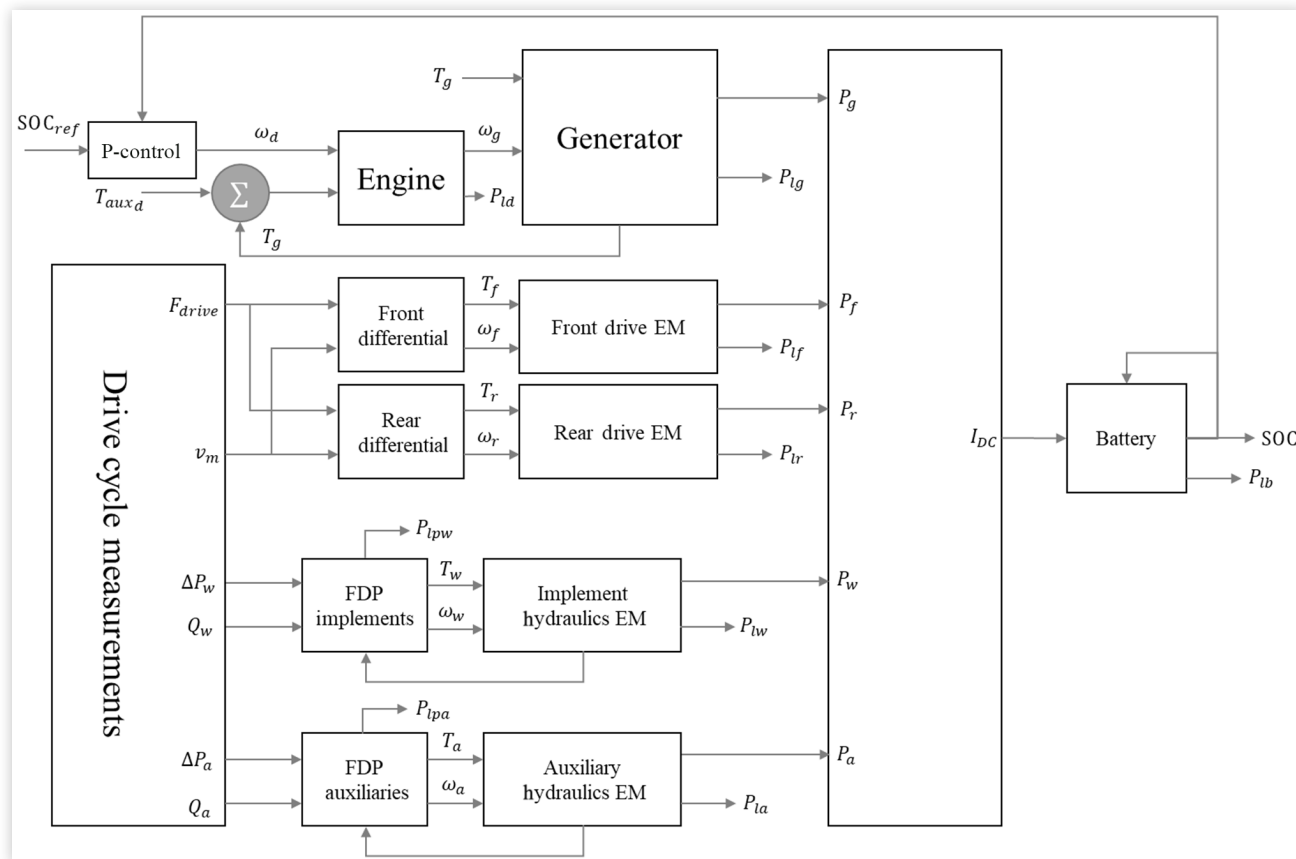


TABLE 1 Simulation parameters of the SEH wheel loader.

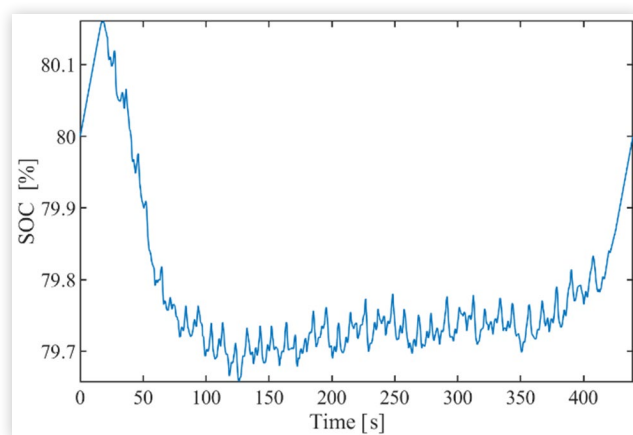
Component	Drive + implements	Value			Unit
		Generator	Auxiliaries		
Electric machines					
Rated/maximum power	65/90	25.3/35	13.9/19.2		kW
Rated/maximum torque	95/200	135/259	28.3/62		Nm
Rated/maximum speed	4200/12,800	1780/6200	4700/9500		RPM
Diesel engine					
Power/speed		91/1900			kW/RPM
Torque/speed		508/1600			Nm/RPM
Battery					
Battery nominal capacity		111			Ah
Maximum current		-150/300			A
Number of cells		7			Series
Nominal voltage		364			V
Fixed displacement pumps		Implements		Auxiliaries	
Pump geometric volume	48		4.5		cc/rev
Pump inertia	0.004		2.8×10^{-4}		kg · m ²
Drivetrain					
Reduction ratio		41.388			uL
Wheel radius		0.51			m

© Mohamed Allam, Orlando Delgado Fernandez, Matti Linjama

the beginning of the simulation are also set at 80% to avoid overcharging of the battery.

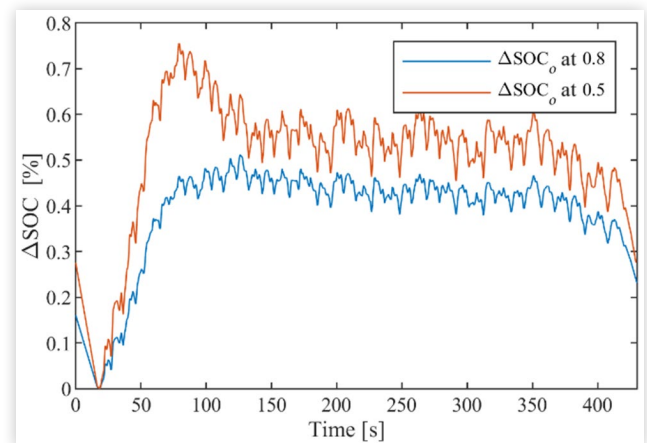
A. System Consumption

The variation of the lithium-ion battery SOC is shown in [Figure 11](#) during the full 440 second cycle. The SOC initially increases as diesel engine is idling and the loading does not start until 20 s and then drops to around 79.7% as the cycle progresses. The small drop in the SOC is attributed to the large capacity of the battery pack, which is sized to accommodate the power requirements of the consumers. At the end, the power from the diesel engine and the generator restores the SOC to its initial value.

FIGURE 11 Battery SOC during the Y-cycle with initial SOC of 80%.

© Mohamed Allam, Orlando Delgado Fernandez, Matti Linjama

It is worth noting that when the cycle was simulated at lower SOC (50%), the performance degraded and the same cycle may discharge the battery more as shown in [Figure 12](#) (showing the drop in battery charge compared to the initial SOC) at lower SOC due to the nonlinear relationship between the OCV and the SOC shown in [Figure 6](#). At lower SOC the OCV of the battery pack is lower, meaning that a higher current is needed to satisfy the requirements of the load cycle. This contributes to more discharge of the battery for the same power demand according to (13). A duration of the current required to complete the Y-cycle is shown in [Figure 13\(a\)](#), and it shows that at lower SOC the current drawn from the battery is slightly higher. Finally, there are higher resistances and losses at lower SOC [34]. This also contributes to more fuel

FIGURE 12 Battery SOC variation with different initial SOC.

© Mohamed Allam, Orlando Delgado Fernandez, Matti Linjama

consumption, which is around 1% more compared to when the battery is charged.

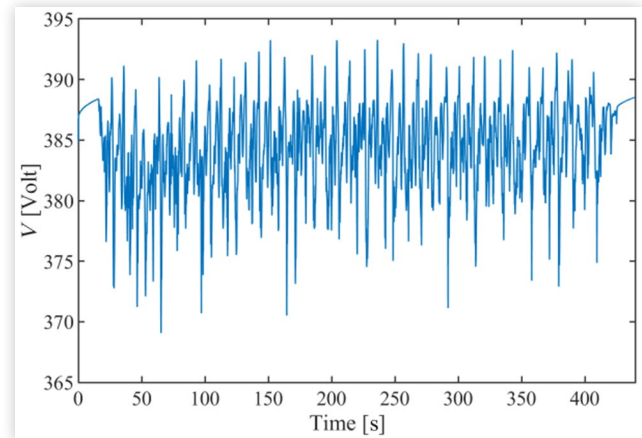
The voltage of the battery is shown in [Figure 14](#) where the terminal voltage varies around 387 V during the cycle with a minimum of around 369.6 V. The maximum voltage drop is caused by the working hydraulics load and the front and rear drive motors while the lowest consumer is the auxiliary's hydraulics motor. The voltage drop from all loads is not enough to trigger the battery management system (BMS) where the maximum current needed for the BMS to intervene is 300 A, which was not exceeded as seen in [Figure 13\(b\)](#). A note worth mentioning is that the pack temperature rose by a few degrees during the seven-minute cycle, which may introduce the need for an active cooling system.

The fluctuation in the battery's terminal voltage is due to the nature of the load profile that contains several transients and is highly dynamic. The maximum voltage drop originates from the extreme condition imposed by the operator during the experiment, where the operator uses maximum accelerator input as well as the hydraulic implements to operate the tilt and lift cylinder all at the same time. This phenomenon occurs at 65 s and can be seen in the implements and drive power required in [Figure 15](#).

The power for each component of the SEH system is shown in [Figure 15](#) where the diesel engine maximum used power is about 26 kW or around 29% of its available power, which indicates that there's a possibility of engine downsizing for this cycle, which is one of the most demanding duty cycles of wheel loaders. The implements, auxiliaries, and drive motors are operating within their nominal power range with some power peaks for a few seconds that could be managed without overheating the electric motors according to the manufacturers' data sheet. The maximum power of the motors could be utilized during transient high-load events such as acceleration, digging, or heavy lifting. Additionally, the battery is operated within its charging/discharging current with space for more extreme loading, especially during acceleration and deceleration. On the other hand, heavy loading from implements or side pumps is mitigated through hydraulic pressure relief valves. Finally, in case of heavy braking where the maximum battery recharge current is exceeded the extra energy could be dissipated using a brake resistor.

On the other hand, the power of the drive electric motors shows possibilities of energy regeneration during the cycle

FIGURE 14 Terminal voltage of the battery during the Y-cycle where the initial state of charge is 80%.



© Mohamed Allam, Orlando Delgado Fernandez, Matti Linjama

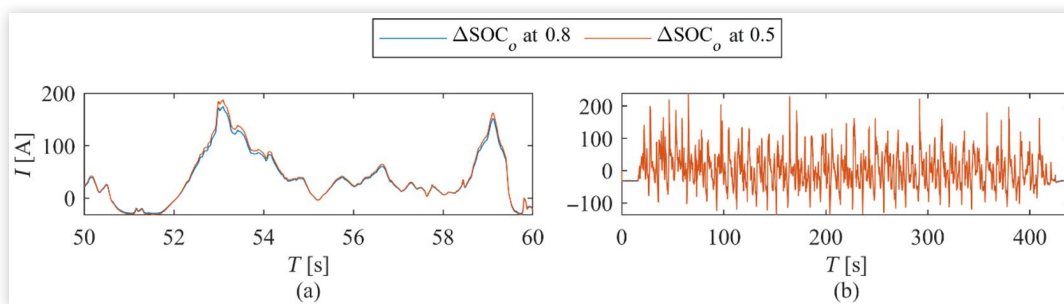
where conventional braking is done in part by the HST but with no regeneration. During the experiment, the wheel loader moves several times forward and in reverse (shown in [Figure 8](#) in the velocity measurements) to finish loading, and several events of regenerative braking are observed. [Figure 16](#) shows a zoomed portion of the SEH drive motors' power with the regeneration highlighted in red and the amount of energy available for regeneration is around 22.48% of the total energy consumed by the drive motors, which is reflected in the fuel consumption.

Some simplifications were made in regenerative braking analysis. For example, regenerative braking maybe limited at lower speeds for safety reasons or when the battery's SOC is at a higher level. In practice, savings due to energy regeneration might be slightly lower due to these limitations. On the other hand, energy regeneration from the implement hydraulics during load lowering for example was not considered, which may improve the energy savings from regeneration [35].

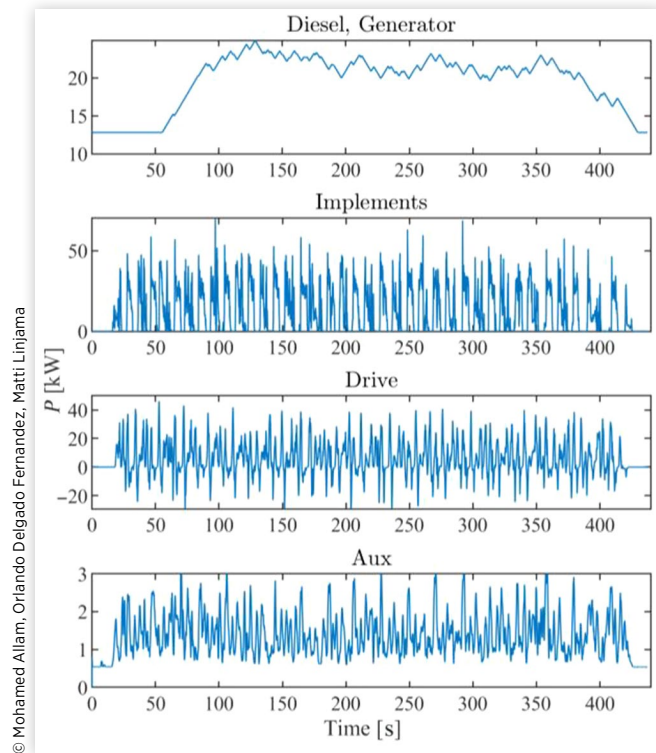
B. Energy and Power Losses

Power losses from the motors, generator, and diesel engine are calculated from the difference between their respective input and output powers. Power losses from the battery are calculated from the resistive losses, which are transformed

FIGURE 13 Current of the battery using different initial SOC's: (a) full cycle; (b) zoomed duration from cycle.



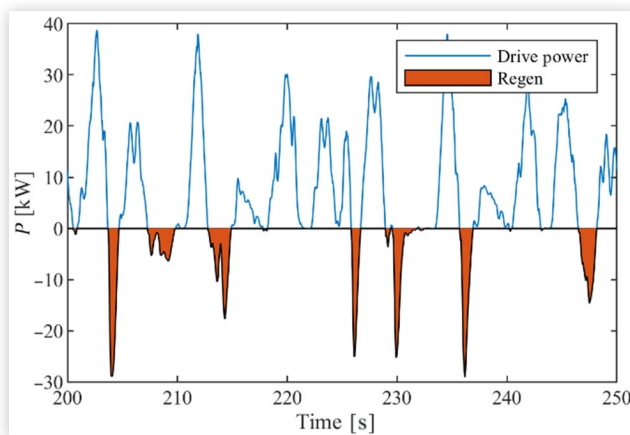
© Mohamed Allam, Orlando Delgado Fernandez, Matti Linjama

FIGURE 15 Power of SEH components.

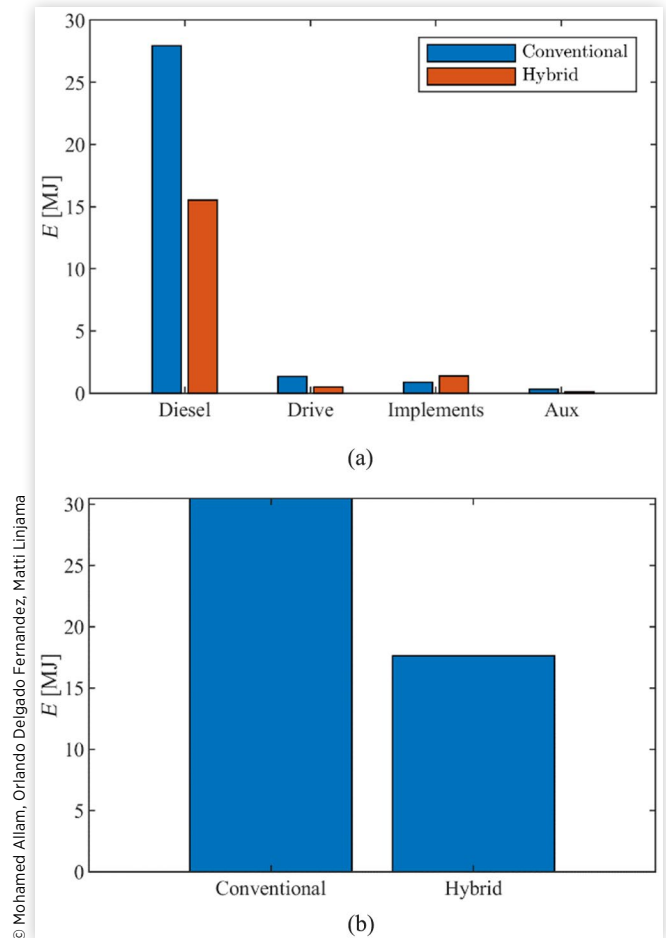
© Mohamed Allam, Orlando Delgado Fernandez, Matti Linjama

into heat energy according to (12). Losses in the hydraulic pumps are calculated using (20), (21). Energy losses are calculated from power losses using the simulation model. Energy losses for a specific system is calculated by adding losses from individual components. Additionally, the energy losses of the SEH machine are the sum of all component losses including diesel engine, electric motors, generator, hydraulic pumps, battery, and inverters while for the conventional machine it is losses from the diesel engine, HST, VDPs, and hydraulic motors.

The energy losses of the powertrain components are detailed in Figure 17(a), and it shows that the diesel engine

FIGURE 16 Battery energy regeneration (zoomed).

© Mohamed Allam, Orlando Delgado Fernandez, Matti Linjama

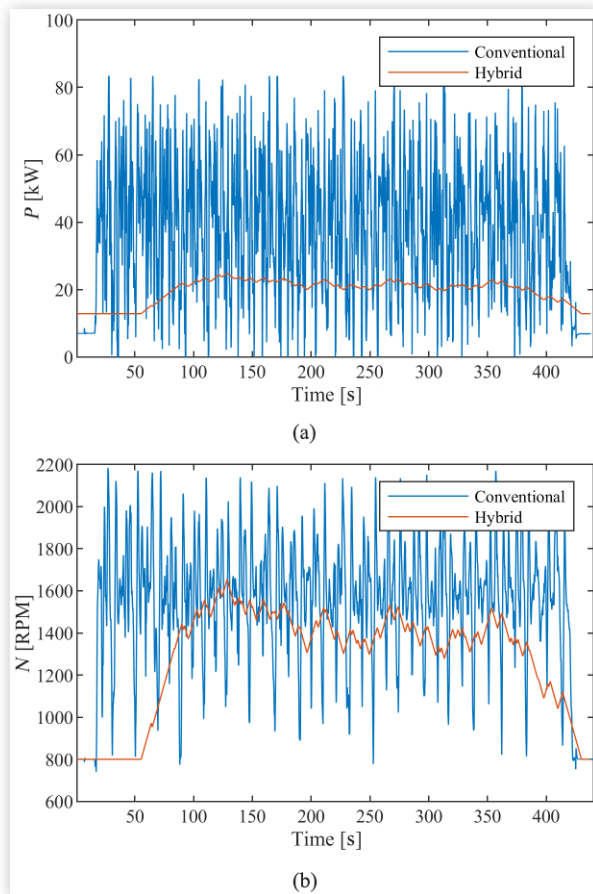
FIGURE 17 Energy losses of the studied powertrains: (a) component losses, (b) total losses.

© Mohamed Allam, Orlando Delgado Fernandez, Matti Linjama

has the highest losses in both the conventional (28 MJ) and SEH architectures with the SEH system showing much lower losses (15.52 MJ). The SEH drive system also shows around 62% less losses (0.5 MJ) as the electric machines are more efficient than the HST (1.3 MJ). On the contrary, the implement hydraulics of the SEH powertrain has 60% higher losses (1.368 MJ) when compared to the conventional system (0.857 MJ) due to the addition of an electric machine to the system and the pump losses difference between a fixed and a variable displacement pump are negligible (conventional machine has a VDP). This disadvantage is shadowed by the savings in the diesel engine consumption. In the auxiliary hydraulics system, the losses are lower in the hybrid architecture (0.124 MJ) since the pump is smaller in size and is fully utilized unlike the conventional system where the pump is connected to the tank and part of the flow is unused (0.336 MJ). Finally, the total energy losses of the two architectures are shown in Figure 17(b) indicating much lower overall energy losses by utilizing a SEH system where the total reduction in energy losses is around 42%.

The SEH system obtains a significant reduction in energy losses by constantly operating the diesel engine at a

FIGURE 18 Diesel engine power in SEH and conventional machines.



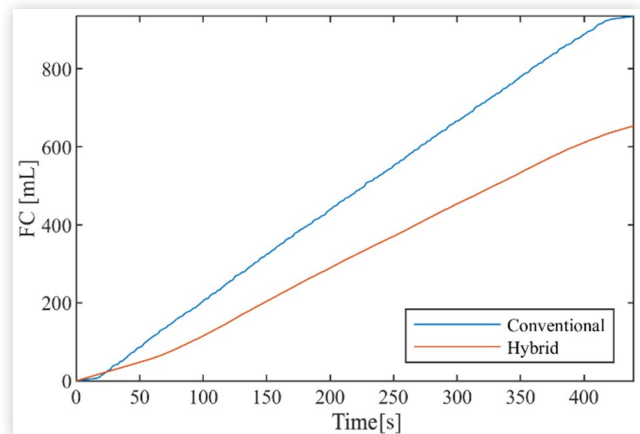
© Mohamed Allam, Orlando Delgado Fernandez, Matti Linjama

high-efficiency zone since it is decoupled from the load. Additionally, in the conventional machine, the diesel engine operates in a transient mode with highly varying speeds, which contributes to even higher losses when compared to a steadier state operation in the SEH machine [36, 37]. Other contributors to the reduction in energy losses include the improved efficiency of the drivetrain and auxiliary systems, but they are not as significant.

C. System Comparison

The SEH powertrain decouples the diesel engine from the load fluctuations allowing it to operate at a speed with lower oscillations and peaks while achieving much better efficiency. Decoupling also reduces the maximum required power from the diesel engine. Figure 18(a) shows the diesel engine power of both machines where the maximum power used by the SEH wheel loader is around 26 kW while the conventional wheel loader requires 83 kW. The mean power of the conventional system is 29.8 kW, where the diesel engine in the conventional powertrain must handle the power transients of different subsystems unlike the SEH powertrain. Figure 18(b) shows the fluctuation of the diesel engine rotational speed in the

FIGURE 19 Fuel consumption of the SEH wheel loader vs the conventional wheel loader.



© Mohamed Allam, Orlando Delgado Fernandez, Matti Linjama

SEH and the conventional system; the SEH system shows much less fluctuations and overall speed than the original machine, which reduces fuel consumption, stresses, and emitted noise levels. A steadier diesel engine operating at lower speed produces less combustion cycles, which results in quieter operation [36, 37].

The SEH diesel engine operation at constant power and higher efficiency zone is reflected in its fuel consumption when compared to the conventional wheel loader. Figure 19 shows the difference between the two systems' fuel consumption where the SEH wheel loader consumes 654 mL of diesel fuel while the conventional system uses 935.3 mL, which translates to a 30% reduction in fuel consumption.

For the auxiliaries' pump, the actual flow rate used by the steering and braking systems was not measured, and hence to compare the two architectures, the pump is assumed to be running at maximum flow for the entirety of the simulation. Although this might overestimate the fuel consumption, it is acceptable in the initial simulation since the auxiliary system power consumption represents 3.5% of the loader's total power consumption. The model was simulated using an estimated work cycle for the auxiliaries' pump and the SEH powertrain was 1% more efficient than when the pump runs at full flow rate. The consumption of the SEH system at the beginning is more than the conventional system as the diesel engine and the generator are recharging the battery while the conventional system is just idling.

Although the SEH loader consumes slightly more fuel compared to the conventional machine initially, this energy is produced and used more efficiently when compared to the conventional machine, which is noticeable in the actual phase of energy consumption during the productivity of the machine. Another assumption made was that the generator is only used at its nominal torque while the manufacturers' data sheet indicates that the maximum torque can be used for short durations without damage to the machine. According to Figure 3, the generator operates at constant nominal torque, which forces the diesel engine into a slightly lower efficiency zone. The performance of the diesel engine can be improved

TABLE 2 Fuel consumption comparison between the series electric hybrid and the conventional architectures.

Architecture	Conventional	SEH
Fuel consumption	935.2 mL	654.3s mL
Improvement	—	30%

© Mohamed Allam, Orlando Delgado Fernandez, Matti Linjama

by operating the generator beyond its nominal torque, but this would come at the cost of overall efficiency and might cause overheating or damage to the generator. Nevertheless, it is possible to improve the consumption more by implementing intelligent control such as a rule-based or an optimization-based energy management strategy for the powertrain to balance the operation of the diesel engine and the generator in terms of overall efficiency and physical constraints.

The overall fuel consumption and the improvement are summarized in [Table 2](#). A 30% improvement means that it is possible to save between 3000 and 30,000 L of diesel per year per machine. These savings have much wider effects than pure reduction in fuel cost, whereby using less fuel the proposed architecture will reduce CO₂ emissions by up to 80 tons per year per machine [38]. It would also reduce the dependence on fossil fuels. Finally, it can improve the lifetime of several components such as braking systems and the diesel engine itself, which in turn would reduce the maintenance cost.

VII. Conclusions

The race toward more efficient working machines is propelling the industry toward developing less-consuming and polluting machines. Electric hybrid machines are one of the main advances in such field and they have the capabilities of significantly improving fuel and energy consumption. This work presented a MATLAB/Simulink model of the purpose-built SEH wheel loader including the diesel engine, electric machines, battery, and fixed displacement pumps. The parameters of the model were identified through measurements when available and from literature as well. The model was used to analyze the studied wheel loader, quantify the losses and efficiency, predict the performance during operation, and the SEH consumption and losses were compared to a conventional machine using real-world duty cycle data that was measured experimentally. Results prove that there is a possibility of at least 30% reduction in fuel consumption using a SEH powertrain for a wheel loader. It also showed that the diesel engine decoupling from the loading conditions transients allows for much more efficient operation where the engine can be run at a more steady speed. The results also showed that it is possible to downsize to a smaller engine as the diesel engine uses only 29% of its maximum available power. Opportunities of energy regeneration during braking were shown where it is possible to regenerate up to 22.48% of the drive system's used power. It is likewise possible to improve the efficiency of the machine by intelligent control of

individual components, which can lead to more fuel and energy savings that can extend the machines' operation time, lifetime, and reduce the overall cost.

The promising saving capabilities of the proposed architecture pave the way toward future development. First, the simulation model requires verification of the machine when constructed. Also, the results showed that there is room for more improvement by employing intelligent control such as optimization-based strategies or predictive control. Additionally, further refinement in component sizing and integration is also possible using the simulation model. The study could also be extended to include the effects of temperature on the performance of such machines given that battery's performance and electric motor's efficiency deteriorate at extreme temperatures. Finally, the scalability and availability of components also pose a significant challenge to industrial implementation where the components used for the machine of the study were not specifically made for heavy-duty machines but rather a collection of different applications, which affects the overall efficiency.

Acknowledgements

This work was co-funded by the Egyptian Cultural Affairs and Missions and Business Finland's Clean Propulsion Technologies project.

Contact Information

Mohamed Allam, corresponding author
mohamed.allam@tuni.fi

References

1. Anon, *Caterpillar Performance Handbook* (Peoria, IL: Caterpillar, 2012)
2. Ahopelto, M., Backas, J., Ghabcheloo, R., and Huhtala, K., "Improved Energy Efficiency and Controllability of Mobile Work Machines by Reduced Engine Rotational Speed," in *ASME 2013 International Mechanical Engineering Congress and Exposition*, San Diego, CA, 2013.
3. Linjama, M., Huova, M., Tammisto, J., Heikkilä, M. et al., "Hydraulic Hybrid Working Machines Project - Lessons Learned," in *Proceedings of the 16th Scandinavian International Conference on Fluid Power (SICFP 2019)*, Tampere, Finland, 2019.
4. Hitachi, "The Wheel Loader of the Future," accessed January 2023, <https://www.hitachicm.eu/iground-control/issue9/en/wheel-loader-of-the-future>.
5. Anon, "Caterpillar Unveils First Hybrid Excavator," Caterpillar Press Release, 2012.

6. Komatsu, "Komatsu WE-Series Wheel Loader," accessed October 2023, <https://www.komatsu.com/en/newsroom/2021/komatsu-we-series-wheel-loader-with-generation-3-hybrid-technology/>.
7. Wang, J., Yang, Z., Liu, S., Zhang, Q. et al., "A Comprehensive Overview of Hybrid Construction Machinery," *Advances in Mechanical Engineering* 8, no. 3 (2016): 1687814016636809, doi:[10.1177/1687814016636809](https://doi.org/10.1177/1687814016636809).
8. Gao, J.-P., Zhu, G.-M.G., Strangas, E.G., and Sun, F.-C., "Equivalent Fuel Consumption Optimal Control of a Series Hybrid Electric Vehicle," *Proceedings of the Institution of Mechanical Engineers, Part D: Journal of Automobile Engineering* 223, no. 8 (2009): 1003-1018, doi:[10.1243/09544070JAUTO1074](https://doi.org/10.1243/09544070JAUTO1074).
9. Barsali, S., Miulli, C., and Possenti, A., "A Control Strategy to Minimize Fuel Consumption of Series Hybrid Electric Vehicles," *IEEE Transactions on Energy Conversion* 19, no. 1 (2004): 187-195, doi:[10.1109/TEC.2003.821862](https://doi.org/10.1109/TEC.2003.821862).
10. Wang, Z., Li, W., and Xu, Y., "A Novel Power Control Strategy of Series Hybrid Electric Vehicle," in *2007 IEEE/RSJ International Conference on Intelligent Robots and Systems*, San Diego, CA, 96-102, 2007, doi:[10.1109/IROS.2007.4399024](https://doi.org/10.1109/IROS.2007.4399024).
11. Chen, B., Evangelou, S.A., and Lot, R., "Series Hybrid Electric Vehicle Simultaneous Energy Management and Driving Speed Optimization," *IEEE/ASME Transactions on Mechatronics* 24, no. 6 (2019): 2756-2767, doi:[10.1109/TMECH.2019.2943320](https://doi.org/10.1109/TMECH.2019.2943320).
12. Katrasnik, T., Trenc, F., and Opresnik, S.R., "Analysis of Energy Conversion Efficiency in Parallel and Series Hybrid Powertrains," *IEEE Transactions on Vehicular Technology* 56, no. 6 (2007): 3649-3659, doi:[10.1109/TVT.2007.901033](https://doi.org/10.1109/TVT.2007.901033).
13. Evangelou, S.A. and Shukla, A., "Advances in the Modelling and Control of Series Hybrid Electric Vehicles," in *2012 American Control Conference (ACC)*, Montreal, QC, Canada, 527-534, 2012, doi:[10.1109/ACC.2012.6315156](https://doi.org/10.1109/ACC.2012.6315156).
14. Hu, X., Murgovski, N., Johannesson, L., and Egardt, B., "Energy Efficiency Analysis of a Series Plug-In Hybrid Electric Bus with Different Energy Management Strategies and Battery Sizes," *Applied Energy* 111 (2013): 1001-1009, doi:[10.1016/j.apenergy.2013.06.056](https://doi.org/10.1016/j.apenergy.2013.06.056).
15. Peng, J., Fan, H., He, H., and Pan, D., "A Rule-Based Energy Management Strategy for a Plug-In Hybrid School Bus Based on a Controller Area Network Bus," *Energies* 8, no. 6 (2015): 5122-5142, doi:[10.3390/en8065122](https://doi.org/10.3390/en8065122).
16. Wang, D., Guan, C., Pan, S., Zhang, M. et al., "Performance Analysis of Hydraulic Excavator Powertrain Hybridization," *Automation in Construction* 18, no. 3 (2009): 249-257, doi:[10.1016/j.autcon.2008.10.001](https://doi.org/10.1016/j.autcon.2008.10.001).
17. Lin, Z., Wang, F., and Xu, B., "Improving Wheel Loader Energy Efficiency with a Series Electric Hybrid Powertrain," in *BATH/ASME 2022 Symposium on Fluid Power and Motion Control*, Bath, UK, 2022, doi:[10.1115/FPMC2022-89099](https://doi.org/10.1115/FPMC2022-89099).
18. Tebaldi, D. and Zanasi, R., "Modeling Control and Simulation of a Series Hybrid Propulsion System," in *2020 IEEE Vehicle Power and Propulsion Conference (VPPC)*, Gijon, Spain, 1-7, 2020, doi:[10.1109/VPPC49601.2020.9330826](https://doi.org/10.1109/VPPC49601.2020.9330826).
19. Donato, T. and Nicolazzo, A., "Preliminary Design of a Hybrid Electric Powertrain for a Earthmoving Machine," *Energy Procedia* 148 (2018): 495-503, doi:[10.1016/j.egypro.2018.08.125](https://doi.org/10.1016/j.egypro.2018.08.125).
20. Lin, T., Lin, Y., Ren, H., Chen, H. et al., "Development and Key Technologies of Pure Electric Construction Machinery," *Renewable and Sustainable Energy Reviews* 132 (2020): 110080, doi:[10.1016/j.rser.2020.110080](https://doi.org/10.1016/j.rser.2020.110080).
21. Hassani, M., "Construction Equipment Fuel Consumption during Idling," MSc thesis, Mälardalen University, Sweden, 2020.
22. Rakopoulos, C., Giakoumis, E., and Michos, C., "Quasilinear versus Filling and Emptying Modelling Applied to the Transient Operation of a Turbocharged Diesel Engine," *International Journal of Vehicle Design* 45 (2007): 150-170, doi:[10.1504/IJVD.2007.013675](https://doi.org/10.1504/IJVD.2007.013675).
23. Immonen, P., "Energy Efficiency of a Diesel-Electric Mobile Working Machine," PhD dissertation, Lappeenranta University of Technology, 2013, ISBN:978-952-265-415-1.
24. Garcés, A., *Modeling, Operation, and Analysis of DC Grids* (London: Elsevier), ISBN:978-0-12-822101-3
25. Pyrhonen, J., Jokinen, T., and Hrabovcova, V., *Design of Rotating Electrical Machines* (West Sussex, UK: John Wiley & Sons, 2009), ISBN:978-0-470-74008-8
26. Plett, G.L., *Battery Management Systems, Volume I: Battery Modeling* (London: Artech House, 2015), ISBN:978-1-63081-023-8
27. Huria, T., Ceraolo, M., Gazzarri, J., and Jackey, R., "High Fidelity Electrical Model with Thermal Dependence for Characterization and Simulation of High Power Lithium Battery Cells," in *2012 IEEE International Electric Vehicle Conference*, Greenville, SC, 1-8, 2012, doi:[10.1109/IEVC.2012.6183271](https://doi.org/10.1109/IEVC.2012.6183271).
28. Huria, T., Jackey, R., Gazzarri, J., Saginaw, M., and Sanghvi, P., "Battery Model Parameter Estimation Using a Layered Technique: An Example Using a Lithium Iron Phosphate Cell," SAE Technical Papers 2013-01-1547, 2013, doi:<https://doi.org/10.4271/2013-01-1547>.
29. Huova, M., Tammisto, J., Linjama, M., and Tervonen, J., "Fuel Efficiency Analysis of Selected Hydraulic Hybrids in a Wheel Loader Application," in *BATH/ASME 2018 Symposium on Fluid Power and Motion Control*, Bath, UK, 2018, doi:[10.1115/FPMC2018-8869](https://doi.org/10.1115/FPMC2018-8869).
30. Filla, R., "Quantifying Operability of Working Machines," PhD thesis, Linköping University, Sweden, 2011, doi:[10.13140/RG.2.1.4702.0004](https://doi.org/10.13140/RG.2.1.4702.0004).
31. Pahkasalo, C. and Sollander, A., "Adaptive Energy Management Strategies for Series Hybrid Electric Wheel Loaders," MSc thesis, Linköping University, Sweden, 2020.
32. Dadhich, S., Bodin, U., and Andersson, U., "Key Challenges in Automation of Earth-Moving Machines," *Automation in Construction* 68 (2016): 212-222, doi:[10.1016/j.autcon.2016.05.009](https://doi.org/10.1016/j.autcon.2016.05.009).

33. Heikkilä, M., Huova, M., Tammisto, J., Linjama, M. et al., "Fuel Efficiency Optimization of a Baseline Wheel Loader and Its Hydraulic Hybrid Variants Using Dynamic Programming," in *BATH/ASME 2018 Symposium on Fluid Power and Motion Control*, Bath, UK, V001T01A024, 2018, doi:10.1115/FPMC2018-8853.
34. Plett, G.L., *Battery Management Systems, Volume II: Equivalent-Circuit Methods* (New York: Artech House, 2015), ISBN:978-1-63081-028-3
35. Qu, S., Fassbender, D., Vacca, A., and Busquets, E., "A High-Efficient Solution for Electro-Hydraulic Actuators with Energy Regeneration Capability," *Energy* 216 (2021): 119291, doi:10.1016/j.energy.2020.119291.
36. Lindgren, M. and Hansson, P.-A., "Effects of Transient Conditions on Exhaust Emissions from Two Non-road Diesel Engines," *Biosystems Engineering* 87, no. 1 (2004): 57-66, doi:10.1016/j.biosystemseng.2003.10.001.
37. Hansson, P., Lindgren, M., Nordin, M., and Pettersson, O., "A Methodology for Measuring the Effects of Transient Loads on the Fuel Efficiency of Agricultural Tractors," *Applied Engineering in Agriculture* 19 (2003): 251, doi:10.13031/2013.13657.
38. Kawamoto, R., Mochizuki, H., Moriguchi, Y., Nakano, T. et al., "Estimation of CO₂ Emissions of Internal Combustion Engine Vehicle and Battery Electric Vehicle Using LCA," *Sustainability* 11, no. 9 (2019): 2690, doi:10.3390/su11092690.
39. Clean Propulsion Technologies, "Summary of the results of WP4 'Multiple power source propulsion'," accessed January 2024, <https://cleanpropulsion.org/arkistot/2148>.

